



www.asianpubs.org

ARTICLE

Investigation of Graphite Oxide and Reduced Graphene Oxide: Magnetic Properties Revisited

Sisir K. Sarkar^{1,2,✉}, M. Ahmed¹,
M.D. Mukadam³ and S.M. Yusuf³

ABSTRACT

The magnetic properties of graphite oxide (GO) and reduced graphene oxide (RGO), synthesized by chemical methods starting from graphite are reported. A weak paramagnetism, below ~ 50 K, has been found for both samples down to 1.6 K, the lowest measured temperature. The magnetization vs. H/T curves follow the Brillouin function behaviour. The reduced graphene oxide sample, which is prepared by chemical reduction followed by thermal annealing showed enhanced magnetization when compared with that of graphene oxide. The observed values of magnetization correspond to defect induced magnetic moments of 1.91×10^{18} and 5.80×10^{18} per g of graphite oxide and reduced graphene oxide respectively. Our results and the contradictory magnetic properties (*i.e.*, para-, superpara-, ferro-, antiferro-magnetic) of grapheme reported in the literature have been discussed on the basis of current understanding of the subject area.

KEYWORDS

Graphite oxide, Reduced graphene oxide, Magnetic properties revisited.

INTRODUCTION

The development of various methods for producing graphene - a 2D array consisting of sp^2 hybridized carbon atoms in a honeycomb lattice - has stimulated a vast amount of research in recent years [1-4]. The first report on synthesis of graphene was by Geim *et al.* [5,6] who produced graphene by micromechanical cleavage from highly oriented pyrolytic graphite (HOPG) using scotch tape. This distinctive structure of graphene imparts it with remarkable properties like high values of Young's modulus (~ 1.1 TPa), thermal conductivity (~ 5,000 W m⁻¹ K⁻¹), mobility of charge carriers (200,000 cm² V⁻¹ s⁻¹) and electron velocity of ~10⁶ m s⁻¹. These unique properties are ideally suited for applications in energy-storage materials, polymer composites, fast electronic devices like transistors, diodes and oscillators. However, from the application point of view, it remains a challenge to produce high-quality graphene on a large scale. Recently several methods like chemical vapour deposition [7,8], decomposition of SiC at higher temperature [9,10] and chemical methods like

Asian Journal of Materials Chemistry

Volume: 1 Year: 2016
Issue: 3-4 Month: July-December
pp: 66-74
DOI: <https://doi.org/10.14233/ajmc.2016.AJMC-P20>

Received: 9 October 2016
Accepted: 2 December 2016
Published: 9 January 2017

Author affiliations:

¹Chemistry Group, Bhabha Atomic Research Centre, Mumbai-400 085, India

²Chemistry Department, S.P. Pune University, Pune-411 007, India

³Solid State Physics Division, Bhabha Atomic Research Centre, Mumbai-400 085, India

✉To whom correspondence to be addressed:

E-mail: sarkarsk@barc.gov.in

Available online at: <http://ajmc.asianpubs.org>

oxidation promoted exfoliation [11,12] have been employed as possible routes for synthesis of graphene. The current state of research indicates that solution based approach involving chemical reduction of graphite oxide (GO), yielding reduced graphene oxide (RGO) or chemically modified graphene (CMG), is simple and has the advantages of being scalable, rapid and cost effective [13,14]. On the other hand, exploring intrinsic magnetism of graphene has been a long standing interest and the magnetic graphene breakthrough could lead to super fast, super efficient electronic devices based on spintronics [15], in which the magnetic properties of a material as well as its electrical charge are manipulated.

While graphite is a three dimensional carbon based material made up of millions of layers of graphene, graphite oxide is a little different. By the oxidation of graphite using strong oxidizing agents, oxygenated functionalities are introduced in the graphite structure. Compared to pristine graphite, graphite oxide (GO) is heavily oxygenated bearing hydroxyl and epoxy groups on sp^3 hybridized carbon on the basal plane, in addition to carbonyl and carboxyl groups located at the sheet edges on sp^2 hybridized carbon. Hence, graphite oxide is highly hydrophilic and readily exfoliated in water, yielding stable dispersion consisting mostly of single layered sheets (graphene oxide). The inter-layer distance between the graphene oxide sheets increases reversibly from 6 to 12 Å with the increasing relative humidity [16]. Several models are still being debated in the literature [17-19] though extensive research has been done to reveal the chemical structure of graphite oxide. It is important to note that although graphite oxide and graphene oxide share similar chemical properties (*i.e.* surface functional group), their structures are different. The pristine graphite sheet is atomically flat with the van der Waals thickness of ~0.34 nm, graphene oxide sheets are thicker due to the displacement of sp^3 hybridized carbon atoms slightly above and below the original graphene plane and presence of covalently bound oxygen atoms. Graphene oxide is a monolayer material produced by the exfoliation of graphite oxide. Li *et al.* [11] and Lotya *et al.* [12] showed that the surface charges on graphene oxide are highly negative when dispersed in water by measuring the zeta potential due to the ionization of the carboxylic acid and the phenolic hydroxyl groups. Therefore, the formation of stable graphene oxide colloids in water was attributed not only to its hydrophilicity but also the electrostatic repulsion.

Reducing graphene oxide to produce reduced graphene oxide is an extremely crucial process as it has a large impact on the quality of the reduced graphene oxide produced and therefore, determines how closely the structure of reduced graphene oxide can match with that of the pristine graphene. Reduced graphene oxide can be considered as ill-defined intermediate between graphene and graphene oxide. Graphene oxide can be reduced by chemical (using various reductants, such as hydrazine, dimethylhydrazine, hydroquinone and NaBH_4), thermal and ultraviolet-assisted electrochemical methods or by combination of these methods to produce reduced graphene oxides whose electrical conductivity could be made comparable with that of graphene [20].

Many experimental and theoretical studies have been carried out to understand the origin and basic mechanism of

the magnetic properties of graphene and related materials. But experimental and theoretical reports on the magnetic properties of graphite oxide (GO) and reduced graphene oxide (RGO) are scanty. As stated earlier, since reduced graphene oxide needs to be prepared starting from graphite *via* the graphite oxide route, a careful study of their magnetic properties is of great interest. However, experimental evidence for magnetism of graphene in the literature remains both scarce and controversial [21-27]. Room temperature (RT) ferromagnetism (FM), a weak paramagnetic (PM), weak superparamagnetism and even a room temperature superconductivity from a water-treated graphite powder had been reported. Presently there have been many theoretical studies [28-37] suggesting that zigzag edges or point defects in graphene as the spin units which should carry magnetic moments. The possible long-range order coupling among them is ferromagnetic or antiferromagnetic, depending on whether the zigzag edges or defects correspond to the same or to different hexagonal sublattice of the graphene lattice, respectively.

As pointed out by Nair *et al.* [21] these divergent and controversial properties could arise from samples which are not mass produced high-purity graphene. Currently, the intrinsic magnetic properties of graphene in finite sizes are far from being understood, therefore, at least tens of milligram-scale amount of high-purity graphene is an essential prerequisite to unravel the intrinsic magnetism data of graphene. In this article, details of the preparation *via* chemical route, characterization and measurements of magnetic properties of the graphite oxide (GO) and reduced graphene oxide (RGO) are presented. Both graphite oxide and reduced graphene oxide exhibit paramagnetic behaviour down to the lowest measured temperature of 1.6 K. The magnetization *vs.* H/T curves follow the Brillouin function behaviour. The reduced graphene oxide sample, which is prepared by chemical reduction followed by thermal annealing showed enhanced magnetization when compared with that of graphite oxide. The observed values of magnetization correspond to defect induced magnetic moments (1.91×10^{18} and 5.80×10^{18} per g of graphite oxide and reduced graphene oxide respectively). The contradictory magnetic properties (*i.e.*, paramagnetic, superparamagnetic, ferromagnetic, antiferromagnetic) of graphene reported in the literature have been discussed on the basis of current understanding of the subject area.

EXPERIMENTAL

Synthesis of graphite oxide: Graphite oxide was synthesized from graphite by the modified Hummers method [38]. First, a 250 mL flask was filled with 2 g of graphite. Then, 50 mL of H_2SO_4 was added to it at room temperature. The above solution was cooled to 0 °C, followed by a slow addition of 7 g of KMnO_4 while maintaining the temperature below 10 °C. After complete addition of KMnO_4 , the temperature was increased to 10 °C. The mixture was stirred for 2 h. An excess water was added into the mixture at 0 °C (ice bath) and then H_2O_2 (30 wt % in water) was added until the effervescence ceases. The graphite oxide powder was washed with copious amount of water and dried under the ambient condition.

The formation of graphite oxide from bulk graphite has recently been shown to proceed through three distinct and independent steps [39]. The first step is conversion of graphite into a stage-1 sulfuric acid-graphite intercalation compound ($\text{H}_2\text{SO}_4\text{-GIC}$). Next stage-1 GIC gets converted into pristine graphite oxide (PGO), which is an oxidized and c-axis ordered form of graphite. This rate-determining step makes the entire process diffusion-controlled and offers greater understanding for the mechanism of graphite oxide formation. Finally pristine graphite oxide gets converted into graphite oxide after exposure to water where there is no remaining c-axis order.

On the basis of the DFT modeling results [40], the significant qualitative differences between graphene monolayer oxidation and graphite surface oxidation has been demonstrated. At the initial oxidation steps for graphite, the epoxy groups transform into hydroxyl and water intercalates under the top layer of graphite. When the graphite surface is more than 60 % oxidized, the vacancy formation and intercalation by larger molecules such as sulfuric acid begin.

The structure of graphite oxide is still elusive today due to its non-stoichiometry and several models have been proposed to elucidate its structure. Although the consensus is that graphene oxide is decorated by epoxies and hydroxyls, which are randomly distributed across the carbon backbone and carbonyls and carboxyls are mainly attached on the edge, some uncertainty still revolves around the morphology of graphite oxide, Near-edge X-ray absorption fine structure (NEXAFS) for the O-K edge suggested that the carbonyls on average are arranged on the carbon layer and there is locally ordered structure from some oxygenated functional groups [41]. A scanning tunnelling microscope (STM) study on oxidized exfoliated graphene sheets showed an ordered structure exists from pure epoxies arranged in a rectangular lattice on both sides of the carbon layer [42].

Synthesis of reduced graphene oxide: 200 mg of dry graphite oxide was dispersed in 200 mL of nanopure water with sonication for 1 h to yield a 1.0 mg/mL colloidal solution. The pH value of this solution was adjusted to 9.5 by 5 wt % sodium carbonate solution. Sodium borohydride (1.6 g) was directly added into 200 mL of the graphene oxide-dispersion under a magnetic stirring and the mixture was kept at 80 °C (reflux) for 4 h with constant stirring. The reduced product was separated by a centrifugation, washing several times with water and vacuum filtration. The sample was dehydrated with concentrated sulfuric acid at 180 °C for 1 h and further annealed at 600 °C in an argon atmosphere for 2 h.

Sodium borohydride is a common reducing agent widely known to synthetic chemists. It is a salt containing a tetrahedral BH_4^- anion, which readily solubilizes in aqueous and alcoholic media. In the presence of an electrophile such as a carbonyl, the borohydride anion readily performs a hydride transfer reaction to result in an oxyanion and an electron deficient BH_3 molecule. Subsequent stabilization of the BH_3 molecule with the oxyanion reinstates the borohydride as a hydride transfer agent. This is ideally the case until all B-H bonds are exhausted in NaBH_4 [43].

The transformation of graphene oxide to graphene often observed by a colour change of the reaction mixture from

brown (of graphene oxide) to black (of graphene) and an increase of hydrophobicity/aggregation of the material as a result of the removal of oxygen containing groups. Electrical conductivity of the reduced graphene oxide is an important indicator evaluating how the sp^2 carbon network gets restored in this structure. Original graphite oxide is an insulator, with a conductivity of around 10^{-7} S m^{-1} . After reduction with NaBH_4 and dehydration by concentrated sulfuric acid, the conductivity of the prepared reduced graphene oxide increased to $1.5 \times 10^3 \text{ S m}^{-1}$ [17-19]. However, it may be noted that reduced graphene oxide structure is different from pristine graphene, even if all oxygen-containing groups are completely removed from the carbon network.

Characterization by XRD, Raman and FTIR: The synthesized samples were characterized by several techniques. The optical absorption spectra clearly showed a weak absorption around 260 nm for graphite oxide, while in reduced graphene oxide we observe higher absorption in the visible region of the spectra which gets red-shifted towards 300 nm. This observation indicates that percolation of the isolated oxidized domains exists within the sheet.

The XRD patterns of graphite oxide and reduced graphene oxide were recorded (Fig. 1). The interlayer distance obtained in graphite oxide was markedly expanded to 8.7 Å ($2\theta = 10.2^\circ$) from 3.34 Å in graphite. The large interlayer distance has been attributed to the formation of hydroxyl, epoxy and carboxyl groups. With reduction, the interlayer distance in the reduced graphene oxide is expected to contract due to the removal of such functional groups. It can be seen that the main peak of graphite oxide has disappeared completely and the reduced graphene oxide peak appears giving the separation between the reduced graphene oxide layers as 3.52 Å.

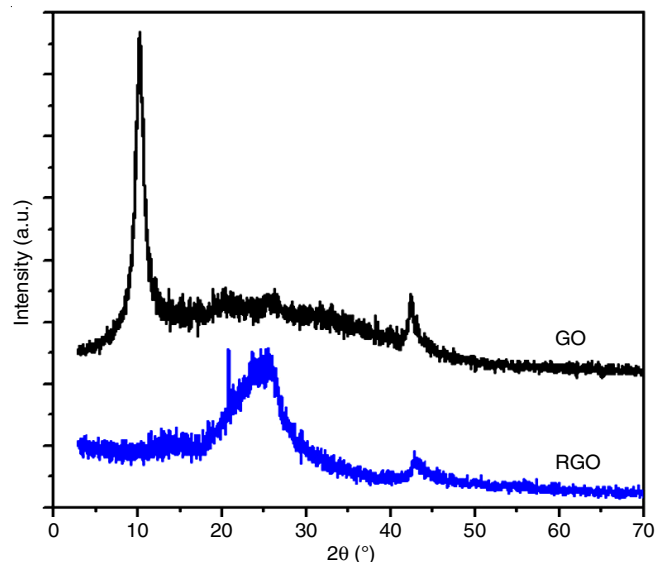


Fig. 1. Comparison of XRD of graphite oxide (GO) and reduced graphene oxide (RGO)

Raman spectroscopy is one of the most powerful and standard non-destructive tools to study graphene based materials. More specifically, reduction of graphite oxide to reduced graphene oxide has been studied more extensively using the Raman spectroscopy to identify the nature of bonding, crystal

structure, disorder defects, doping concentration, electron-phonon interaction, *etc.* [44-46]. A typical Raman spectrum of graphene material, exhibits two prominent broad D ($\sim 1345\text{ cm}^{-1}$) and G ($\sim 1590\text{ cm}^{-1}$) peaks corresponding to the first order scattering of E_{2g} mode (in plane vibrations of sp^2 carbon atoms) and defect induced modes (breathing mode of sp^3 carbon), respectively. In addition to D and G peaks, weak Raman bands at $\sim 2700\text{ cm}^{-1}$ and $\sim 2900\text{ cm}^{-1}$ correspond to overtone 2D and (D+G) peaks, respectively. The 2D peak is attributed to double resonance transitions resulting in the production of two phonons with opposite momentum. Further, unlike D peak, which is Raman active only in the presence of defects, 2D peak is active even in absence of any defects.

Raman spectra of the graphite oxide and reduced graphene oxide are shown in Fig. 2. Compared with graphite oxide, the band of reduced graphene oxide is red shifted from 1590 to 1576 cm^{-1} . This is attributed to the recovery of hexagonal network (sp^2 domains). Meanwhile, the ratio of the intensity of the D-band to that of the G-band, (I_D/I_G) (which reveals the sp^2/sp^3 ratio) of graphite oxide (0.97) is smaller than those of reduced graphene oxide (1.08). The variation of these I_D/I_G ratios is related to structural distortion, surface rippling and wrinkle-structures, which are reported in the SEM images and are formed in the graphene lattice by the restoration of C sp^2 bonds and de-oxidation upon reduction, such that the ratio (I_D/I_G) is sensitive to thermal reduction. The increment of I_D/I_G ratio is in accordance with the several other studies on reduction of graphite oxide.

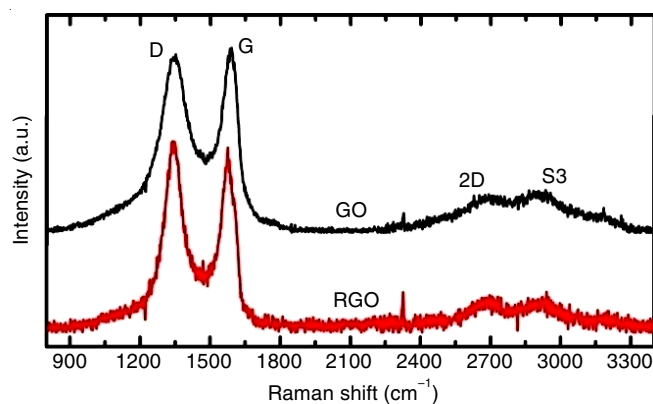


Fig. 2. Comparison of Raman spectra of graphite oxide (GO) and reduced graphene oxide (RGO)

The reduction of the graphite oxide was further investigated by a FT-IR spectroscopy to trace the alteration of chemical bonds in the reduced graphene oxide. Fig. 3 shows the FT-IR spectra of the graphite oxide and reduced graphene oxide. The spectrum of graphite oxide illustrates the presence of the C=O bond in carboxylic acid and carbonyl moieties ($\nu_{C=O}$ at 1719 cm^{-1}), C-OH (ν_{C-OH} at 1394 cm^{-1}), C-O-C (ν_{C-O-C} at 1170 cm^{-1}) and C-O (ν_{C-O} at 1059 and 860 cm^{-1}) [36]. The peak at 1610 cm^{-1} may arise from the skeletal vibrations of the unoxidized graphitic domains or stretching deformations of the intercalated water. Reduced graphene oxide shows a much clearer spectrum, compared to that of the graphite oxide, with the greatly diminished peaks at 1719 , 1394 , 1170 and 1059 cm^{-1} , which indicates the removal of oxygen functional groups,

such as carboxylic acid, epoxide and hydroxyl groups upon reduction. These results once again confirm the reduction of the graphite oxide.

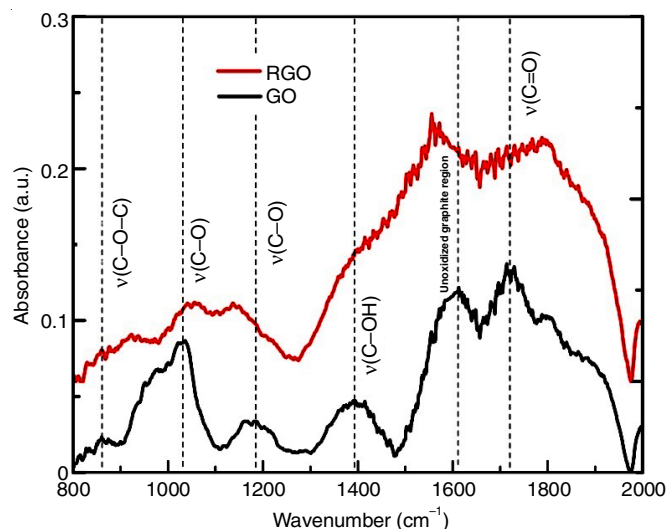


Fig. 3. FT-IR spectra of graphite oxide (GO) and reduced graphene oxide (RGO)

RESULTS AND DISCUSSION

Magnetic measurements: The dc magnetization measurements were carried out, using a vibrating sample magnetometer (Cryogenic, UK), as a function of temperature and magnetic field. For temperature dependent zero-field-cooled magnetization (M_{ZFC}) measurements, the sample was first cooled from room temperature down to 1.6 K in zero external field. After applying the magnetic field at 1.6 K , the magnetization was measured in the warming cycle with field on. Whereas, for temperature dependent field-cooled magnetization (M_{FC}) measurements, the sample was cooled from room temperature down to 1.6 K in the same field (measuring field in the ZFC case) and M_{FC} was measured in the warming cycle keeping the field on. Magnetization as a function of applied field over the all four quadrants with a maximum field of $\pm 50\text{ kOe}$ was measured after cooling the sample to the measurement temperature (1.6 and 5 K) under zero field.

Fig. 4(a) shows the M_{ZFC} and M_{FC} dc magnetization as a function of temperature under 1 kOe magnetic field for the graphite oxide. A diamagnetic behaviour (negative magnetization) has been found over the temperature range of 300 - 50 K . However, a clear indication of the presence of a paramagnetic signal (positive magnetization) has been observed below $\sim 50\text{ K}$ where the magnetization increases steadily with decreasing temperature. No branching between the M_{ZFC} vs. T and M_{FC} vs. T curves has been observed. The observed temperature dependence of magnetization obeys the Curie law indicating a true paramagnetic behaviour of the sample down to the lowest measured temperature of 1.6 K . The magnetization curves as a function of magnetic field at 1.6 and 5 K for the sample are shown in Fig. 4(b). A significant diamagnetic contribution is quite evident from the $M(H)$ curves. Fig. 4(c) shows the $M(H)$ curves after correcting for the diamagnetic contribution as

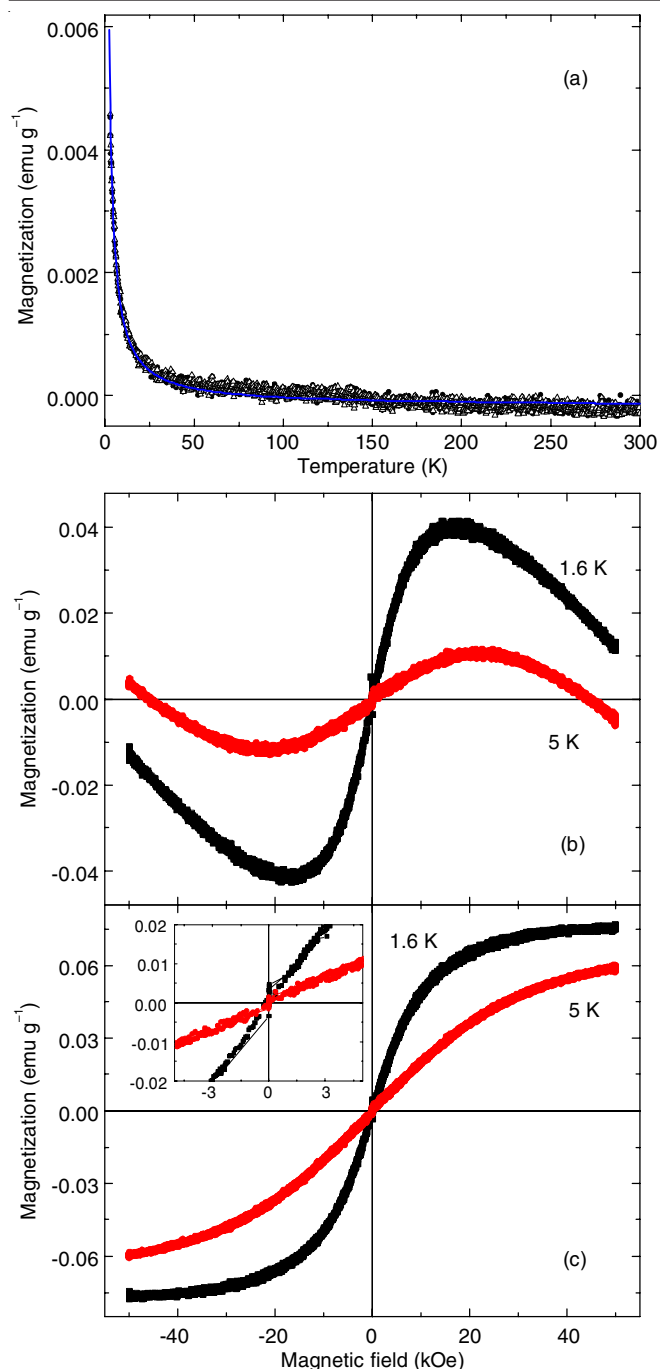


Fig. 4. (a) ZFC (solid circles) and FC (open triangles) Magnetization as a function of temperature under 1 kOe magnetic field for the graphite oxide sample. Solid line is the Curie law fit. The diamagnetic contribution is also considered for the fitting. (b) The measured field dependence of dc magnetization at 1.6 and 5 K for the graphite oxide sample. (c) dc magnetization at 1.6 and 5 K for graphite oxide after correcting for the diamagnetic contribution. The inset enlarges the low field region of the $M(H)$ curves

obtained from the $M(H)$ study at room temperature. The s-shape nature of the $M(H)$ curves in Fig. 4(c), with a tendency towards its saturation at 1.6 K, is evident. Besides, no hysteresis has been observed down to 1.6 K. The observed $M(H)$ behaviour is, therefore, consistent with the paramagnetic behaviour found in Fig. 4(a). However, it is interesting to note here that a moderate magnetic field of 50 kOe is nearly adequate to saturate the paramagnetic moments of the sample.

Fig. 5(a), 5(b) and 5(c) show the magnetization as a function of temperature and magnetic field for the reduced graphene oxide sample. The magnetic behaviour of the sample is similar to that of graphite oxide, however, with a significantly enhanced signal. For graphite oxide, at the lowest temperature of 1.6 K, the observed maximum magnetization is ~ 0.075 emu/g, whereas it is 0.17 emu/g for the reduced graphene oxide sample. Fig. 6(a) and 6(b) show the magnetization as a function

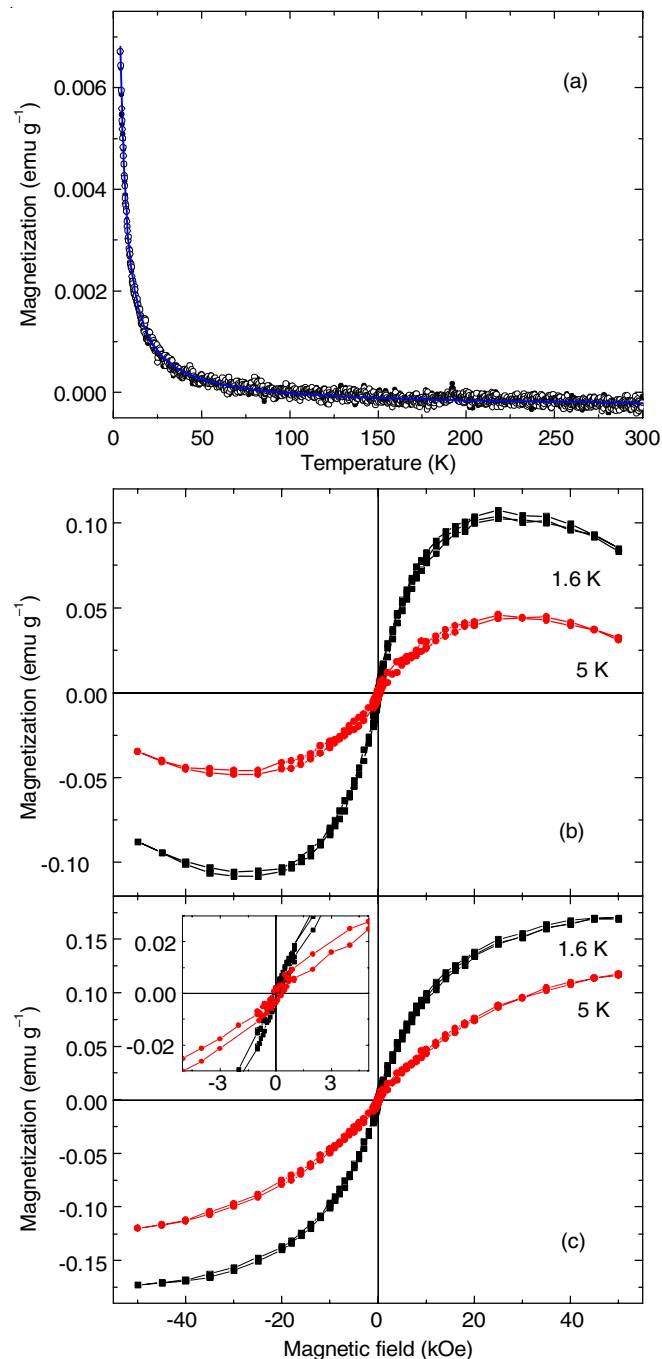


Fig. 5. (a) ZFC (solid circles) and FC (open triangles) magnetization as a function of temperature under 1 kOe magnetic field for reduced graphene oxide. Solid line is the Curie law fit. The diamagnetic contribution is also considered for the fitting. (b) measured field dependence of dc magnetization at 1.6 and 5 K for reduced graphene oxide and (c) magnetization at 1.6 and 5 K for reduced graphene oxide after correcting for the diamagnetic contribution. The inset enlarges the low field region of the $M(H)$ curves

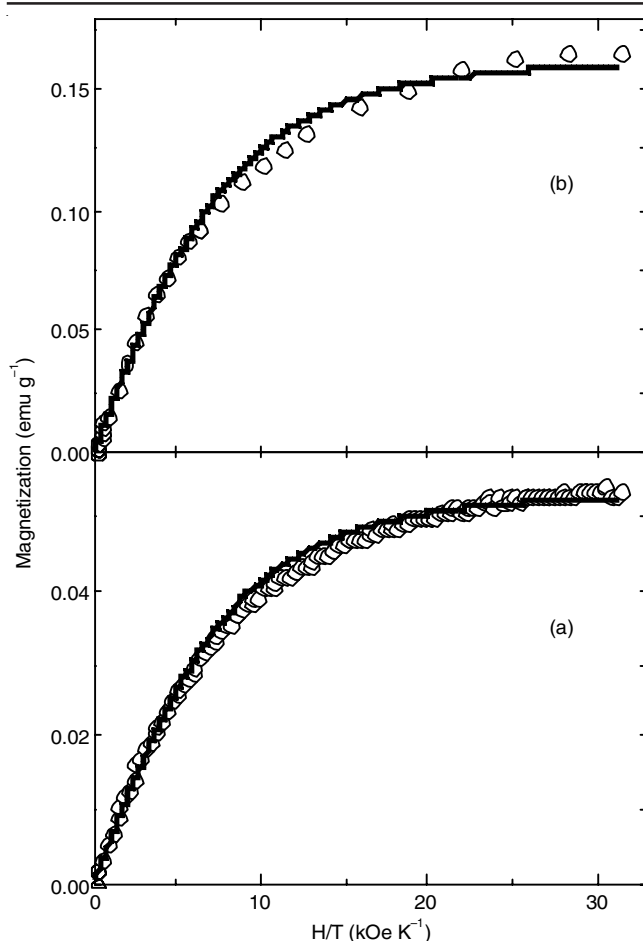


Fig. 6. Magnetization as a function of H/T at 1.6 K for (a) graphene oxide (a) and (b) reduced graphene oxide samples. The solid lines are fits with the Brillouin function

of reduced field (H/T) for both graphene oxide and reduced graphene oxide samples. The observed magnetization is fitted using the Brillouin function:

$$M = NgJ\mu_B \left\{ \frac{2J+1}{2J} \operatorname{ctnh} \left(\frac{(2J+1)x}{2J} \right) - \frac{1}{2J} \operatorname{ctnh} \left(\frac{x}{2J} \right) \right\}$$

where $x = g J m_B H/k_B T$, is the ratio of the Zeeman energy of the magnetic moment in the effective field H_e to the thermal energy, the effective field $H_e = H + H_m$, where the H_m is the molecular field proportional to magnetic moment M , k_B is the Boltzmann constant, g is the Lande g factor, J is the angular momentum number and N is the number of present magnetic moments. Assuming $g = 2$, the best fit with the Brillouin function is obtained with $J = 3/2$ for both samples. The values of N are derived to be 1.91×10^{18} and 5.80×10^{18} per g for the graphite oxide and reduced graphene oxide samples, respectively. These lower values of N (induced spin centers) are typical of a spin system with a weak paramagnetic behaviour, while representative materials with a strong paramagnetic behaviour would have N values in the range of 10^{21} - 10^{22} . The derived value of $g (= 2)$ indicates that spin only moments (*i.e.* without any orbital moments) contribute to the magnetism of these samples. We have determined magnetic impurities in the sample to be lower than 10 ppm level using X-ray fluorescence spectroscopy and verified that the paramagnetic behaviour is quite reproducible.

Now we discuss the possible mechanism for the observed magnetic behaviour of the studied samples. A defect free graphene plane *i.e.*, a single layer of graphite should be diamagnetic since graphite itself is diamagnetic. Wang *et al.* [23] have reported room temperature ferromagnetism in graphene while Matte *et al.* [24] have found the presence of both ferromagnetic and anti-ferromagnetic features in graphene. But Sepioni *et al.* [25] have found no ferromagnetism in graphene at any temperature down to 2 K, but a strong diamagnetism above 50 K (similar to graphite) and a weak paramagnetism below 50 K. Judging from these reports, it appears that the graphene samples, prepared by various methods, can behave differently and these observations could be better represented by the nature of defects in these samples. A real graphene has several defects like topological defects (pentagons, heptagons in their combination), atomic defects (vacancies like missing C-atoms, adatoms, *etc.*) and extended defects (zigzag edges, cracks, *etc.*). Further it may be mentioned that a real graphene is also not perfectly planar; rather corrugations, ripples, wrinkles *etc.* occur on it. Literature provides extensive theoretical and experimental studies on magnetic behaviour of graphene based on both defects and zigzag states.

Yazyev *et al.* [32] have shown that a magnetic moment of about one Bohr magneton can develop due to the defect induced extended states for one vacancy defect or one hydrogen chemisorption defect. Yazyev [28] has also shown that single-atom defects can induce ferromagnetism in the disordered graphene and proton-irradiated graphite. Many theoretical studies revealed that the defects could induce a magnetic moment in a small defect region of graphene. If they are coupled by RKYY or any other exchange interactions ferromagnetism can appear. If they are well separated so that they are not coupled, a weak or strong paramagnetism can appear. Though the mechanism of strong exchange interaction required for the magnetic moments to appear at room temperature is not clearly understood, the magnetic behaviour should depend on the concentration of the defects in graphene. It appears that the concentrations of the defects in the graphene samples of references [23 and 24] are high, while it is small for the sample studied [25].

Applying Lieb theorem [50] the epoxide groups cannot induce local magnetic moments, but the O atom of the hydroxyl group bonded to only one C atom of either sublattice can induce local magnetic moments. Hence such moments, developed due to the hydroxyl groups, are to be considered along with the moments developed due to vacancy defects. If these moments are well separated so that they do not interact, paramagnetism is expected to appear, which we have observed for the graphite oxide and annealed reduced graphene oxide samples. We added here that besides the preparation procedure, the defects in the graphite oxide and reduced graphene oxide very much depend on the starting graphite material used during the preparation. As a consequence, the magnetic properties, originated from the defects, vary from sample to sample.

However, numerous reports have suggested that oxygen-containing [functional groups *e.g.*, carbonyl (C=O), carboxyl (-COOH), epoxy (C-O-C), *etc.*] and/or hydroxyl (-OH) groups are responsible for magnetism in graphene and related materials [51-57]. Boukhvalov *et al.* [51,52] suggested that the hydroxyl

clusters favours magnetism in graphene and the most stable magnetic configuration in graphene sheets involve the high-spin hydroxyl groups that are formed on top of wrinkles or ripples. Santos *et al.* [53] applied density functional theory to calculate the local spin moments of the carboxyl and hydroxyl groups as 1 and 0.56 μB respectively that are adsorbed on the surface of graphene. Similar DFT calculation by Wang *et al.* [54] further revealed that the hydroxyl group is mostly responsible for ferromagnetism in graphite oxide and they further proposed that the presence of two hydroxyl groups bound to non-neighbouring carbon atoms separated by one carbon atom favours the magnetic moment in graphene oxide.

Various functionalized groups ($-\text{OH}$, $-\text{O}-$, $-\text{COOH}$, $\text{C}=\text{O}$, *etc.*) enter into the graphene skeleton, breaking the π bond of graphene structure [58] during the oxidation process, but the exact decoration of the functionalized groups on the graphene skeleton remain uncertain. However, NMR study of graphene oxide has shown that the carbonyl groups are located in the periphery of the graphene oxide sheet [59,60]. Therefore, it may be inferred that only hydroxyl ($-\text{OH}$) and epoxy ($-\text{O}-$) groups are abundant in the interior region of the graphene sheets. After chemical reduction process, it is expected that magnetic moment of graphene oxide to decrease due to removal of such groups. On annealing reduced graphene oxide the concentration of epoxy groups reduces further and the magnetic moment should decrease, but we have observed an increase in moment after annealing reduced graphene oxide at 600 °C. This shows that apart from removing the functional groups from graphite oxide annealing does something more. The π electrons are energetically degenerate at the zigzag edges and have highly localized edge states. These edge states are populated with the same spin to minimize the Coulomb repulsion energy, leading to large moments at the zigzag edge boundary [61-68]. Upon chemical reduction followed by annealing at 600 °C, the density of wrinkles in the graphene oxide sheet decreased owing to the removal of many epoxy groups, increasing the number of zigzag edges/edge states, causing annealed reduced graphene oxide to have greater magnetism than graphite oxide.

Element-specific high-spatial-resolution chemical analysis is a desirable tool for directly examining the role of oxygen-containing and hydroxyl groups in particular regions and to elucidate the difference between chemical states in specific (wrinkle or flat) regions on the surfaces of graphite oxide and reduced graphene oxide. Synchrotron-based X-ray microscopic and spectroscopic techniques have been applied on graphite oxide, photo-thermal moderately reduced graphene oxide (M-RGO) and heavily reduced graphene oxide (H-RGO) including scanning transmission X-ray microscopy (STXM), X-ray absorption near-edge structure (XANES) spectroscopy, valence-band photoemission spectroscopy (VB-PES) and X-ray magnetic circular dichroism (XMCD) [69]. Element-specific XMCD provides evidence of ferromagnetic behaviour in graphite oxide. The results of C K-edge STXM-XANES provide clear evidence that the higher number of C 2p(σ^*)-derived defect/vacancies states, rather than of the C 2p(π^*) states are bound with oxygen-containing and/or hydroxyl groups on the graphite oxide surface. This feature is related to the change of magnetic behaviour of ferromagnetic graphite oxide to that

of paramagnetic moderately reduced graphene oxide and heavily reduced graphene oxide.

We may add here that the formation of magnetic moments due to vacancies/defects in the structure has been reported for other class of materials as well. For example, we have shown that either presence or absence of ferromagnetic behaviour for the transition element doped semiconducting materials, such as GaN and ZnO, with $\sim 5\%$ of Mn doping where vacancy plays an important role in establishing magnetic order [70] and defect-mediated magnetism in ZnO and carbon-based materials [71]. Ferromagnetism as a universal feature of nanoparticles of the otherwise nonmagnetic oxides, copper oxide nanoparticles, in pure Y_2O_3 nanoparticles has also been reported [72].

Conclusion

We have investigated magnetic properties of the graphite oxide and reduced graphene oxide that were synthesized by chemical methods starting from graphite. A weak paramagnetism, noticeable below $\sim 50\text{ K}$, has been found for both samples down to 1.6 K, the lowest measured temperature. The magnetization *vs.* H/T curves follow the Brillouin function behaviour. The reduced graphene oxide sample prepared by chemical reduction followed by thermal annealing showed enhanced magnetization when compared with that of graphite oxide. The observed values of magnetization correspond to defect induced magnetic moments of 1.91×10^{18} and 5.80×10^{18} per g of graphite oxide and reduced graphene oxide respectively. The enhanced magnetization of the annealed reduced graphene oxide, compared to that of graphite oxide, is consistent with the current understanding of the subject area. It is also discussed here that the contradictory magnetic properties (*i.e.*, para-, superpara-, ferro-, antiferro-magnetic) of graphene reported in the literature on the basis of both defects and zigzag states. It is believed that further studies by tuning disorder and vacancies (similar to graphene) would establish the true nature of the magnetic states in graphite oxide and reduced graphene oxide.

ACKNOWLEDGEMENTS

The authors acknowledge to S.N. Achary, Bhabha Atomic Research Centre, Mumbai, India for XRD analysis and Salil K. Sarkar, former Prof. Presidency University, Kolkata, India for useful discussion. SKS would like to thank the DAE for the award of the Raja Ramanna fellowship.

REFERENCES

1. C.N.R. Rao, H.S.S.R. Matte, K.S. Subrahmanyam and U. Maitra, *Chem. Sci.*, **3**, 45 (2012); <https://doi.org/10.1039/C1SC00726B>.
2. A.K. Geim and K.S. Novoselov, *Nat. Mater.*, **6**, 183 (2007); <https://doi.org/10.1038/nmat1849>.
3. C.N.R. Rao, A.K. Sood, K.S. Subrahmanyam and A. Govindaraj, *Angew. Chem. Int. Ed.*, **48**, 7752 (2009); <https://doi.org/10.1002/anie.200901678>.
4. E.P. Randviir, D.A.C. Brownson and C.E. Banks, *Mater. Today*, **17**, 426 (2014); <https://doi.org/10.1016/j.mattod.2014.06.001>.
5. K.S. Novoselov, A.K. Geim, S.V. Morozov, D. Jiang, M.I. Katsnelson, I.V. Grigorieva, S.V. Dubonos and A.A. Firsov, *Nature*, **438**, 197 (2005); <https://doi.org/10.1038/nature04233>.
6. K.S. Novoselov, A.K. Geim, S.V. Morozov, D. Jiang, Y. Zhang, S.V. Dubonos, I.V. Grigorieva and A.A. Firsov, *Science*, **306**, 666 (2004); <https://doi.org/10.1126/science.1102896>.

7. A. Reina, X. Jia, J. Ho, D. Nezhich, H. Son, V. Bulovic, M. Dresselhaus and J. Kong, *Nano Lett.*, **9**, 30 (2009); <https://doi.org/10.1021/nl801827v>.
8. G.-H. Lee, R.C. Cooper, S.J. An, S. Lee, A. van der Zande, N. Petrone, A.G. Hammerberg, C. Lee, B. Crawford, W. Oliver, J.W. Kysar and J. Hone, *Science*, **340**, 1073 (2013); <https://doi.org/10.1126/science.1235126>.
9. J. Hass, R. Feng, J.E. Millán-Otoya, X. Li, M. Sprinkle, P.N. First, W.A. de Heer, E.H. Conrad and C. Berger, *Phys. Rev. B*, **75**, 214109 (2007); <https://doi.org/10.1103/PhysRevB.75.214109>.
10. V.Y. Aristov, G. Urbanik, K. Kummer, D.V. Vyalikh, O.V. Molodtsova, A.B. Preobrajenski, A.A. Zakharov, C. Hess, T. Hänke, B. Büchner, I. Vobornik, J. Fujii, G. Panaccione, Y.A. Ossipyan and M. Knupfer, *Nano Lett.*, **10**, 992 (2010); <https://doi.org/10.1021/nl904115h>.
11. D. Li, M.B. Müller, S. Gilje, R.B. Kaner and G.G. Wallace, *Nat. Nanotechnol.*, **3**, 101 (2008); <https://doi.org/10.1038/nnano.2007.451>.
12. M. Lotya, P.J. King, U. Khan, S. De and J.N. Coleman, *ACS Nano*, **4**, 3155 (2010); <https://doi.org/10.1021/nn1005304>.
13. M.J. Allen, V.C. Tung and R.B. Kaner, *Chem. Rev.*, **110**, 132 (2010); <https://doi.org/10.1021/cr900070d>.
14. S. Park and R.S. Ruoff, *Nat. Nanotechnol.*, **4**, 217 (2009); <https://doi.org/10.1038/nnano.2009.58>.
15. O.V. Yazyev, *Rep. Prog. Phys.*, **73**, 056501 (2010); <https://doi.org/10.1088/0034-4885/73/5/056501>.
16. A. Buchsteiner, A. Lerf and J. Pieper, *J. Phys. Chem. B*, **110**, 22328 (2006); <https://doi.org/10.1021/jp064113z>.
17. S. Mao, H. Pu and J. Chen, *RSC Adv.*, **2**, 2643 (2012); <https://doi.org/10.1039/c2ra00663d>.
18. D.R. Dreyer, S. Park, C.W. Bielawski and R.S. Ruoff, *Chem. Soc. Rev.*, **39**, 228 (2010); <https://doi.org/10.1039/B917103G>.
19. W. Gao, L.B. Alemany, L. Ci and P.M. Ajayan, *Nat. Chem.*, **1**, 403 (2009); <https://doi.org/10.1038/nchem.281>.
20. Y. Zhu, S. Murali, W. Cai, X. Li, J.W. Suk, J.R. Potts and R.S. Ruoff, *Adv. Mater.*, **22**, 3906 (2010); <https://doi.org/10.1002/adma.201001068>.
21. R.R. Nair, M. Sepioni, I.-L. Tsai, O. Lehtinen, A.V. Krashennnikov, J. Keinonen, T. Thomson, A.K. Geim and I.V. Grigorieva, *Nat. Phys.*, **8**, 199 (2012); <https://doi.org/10.1038/nphys2183>.
22. J. Cervenka, M.I. Katsnelson and C.F.J. Flipse, *Nat. Phys.*, **5**, 840 (2009); <https://doi.org/10.1038/nphys1399>.
23. Y. Wang, Y. Huang, Y. Song, X. Zhang, Y. Ma, J. Liang and Y. Chen, *Nano Lett.*, **9**, 220 (2009); <https://doi.org/10.1021/nl802810g>.
24. H.S.S.R. Matte, K.S. Subrahmanyam and C.N.R. Rao, *J. Phys. Chem. C*, **113**, 9982 (2009); <https://doi.org/10.1021/jp903397u>.
25. M. Sepioni, R.R. Nair, S. Rablen, J. Narayanan, F. Tuna, R. Winpenny, A.K. Geim and I.V. Grigorieva, *Phys. Rev. Lett.*, **105**, 207205 (2010); <https://doi.org/10.1103/PhysRevLett.105.207205>.
26. T. Scheike, W. Böhlmann, P. Esquinazi, J. Barzola-Ququia, A. Ballestar and A. Setzer, *Adv. Mater.*, **24**, 5826 (2012); <https://doi.org/10.1002/adma.201202219>.
27. S.K. Sarkar, K.K. Raul, S.S. Pradhan, S. Basu and A. Nayak, *Physica E*, **64**, 78 (2014); <https://doi.org/10.1016/j.physe.2014.07.014>.
28. O.V. Yazyev, *Phys. Rev. Lett.*, **101**, 037203 (2008); <https://doi.org/10.1103/PhysRevLett.101.037203>.
29. O.V. Yazyev and M.I. Katsnelson, *Phys. Rev. Lett.*, **100**, 047209 (2008); <https://doi.org/10.1103/PhysRevLett.100.047209>.
30. D. Soriano, F. Muñoz-Rojas, J. Fernández-Rossier and J.J. Palacios, *Phys. Rev. B*, **81**, 165409 (2010); <https://doi.org/10.1103/PhysRevB.81.165409>.
31. V.L.J. Joly, K. Takahara, K. Takai, K. Sugihara, T. Enoki, M. Koshino and H. Tanaka, *Phys. Rev. B*, **81**, 115408 (2010); <https://doi.org/10.1103/PhysRevB.81.115408>.
32. O.V. Yazyev and L. Helm, *Phys. Rev. B*, **75**, 125408 (2007); <https://doi.org/10.1103/PhysRevB.75.125408>.
33. J. Jung, T. Pereg-Barnea and A.H. MacDonald, *Phys. Rev. Lett.*, **102**, 227205 (2009); <https://doi.org/10.1103/PhysRevLett.102.227205>.
34. M. Fujita, K. Wakabayashi, K. Nakada and K. Kusakabe, *J. Phys. Soc. Jpn.*, **65**, 1920 (1996); <https://doi.org/10.1143/JPSJ.65.1920>.
35. Y.C. Ma, P.O. Lehtinen, A.S. Foster and R.M. Nieminen, *New J. Phys.*, **6**, 68 (2004); <https://doi.org/10.1088/1367-2630/6/1/068>.
36. L. Chen, L. Guo, Z. Li, H. Zhang, J. Lin, J. Huang, S. Jin and X. Chen, *Sci. Rep.*, **3**, 2599 (2013); <https://doi.org/10.1038/srep02599>.
37. D. Lee, J. Seo, X. Zhu, J.M. Cole and H. Su, *Appl. Phys. Lett.*, **106**, 172402 (2015); <https://doi.org/10.1063/1.4919529>.
38. S. Stankovich, D.A. Dikin, R.D. Piner, K.A. Kohlhaas, A. Kleinhammes, Y. Jia, Y. Wu, S.T. Nguyen and R.S. Ruoff, *Carbon*, **45**, 1558 (2007); <https://doi.org/10.1016/j.carbon.2007.02.034>.
39. A.M. Dimiev and J.M. Tour, *ACS Nano*, **8**, 3060 (2014); <https://doi.org/10.1021/nn500606a>.
40. D.W. Boukhvalov, *J. Phys. Chem. C*, **118**, 27594 (2014); <https://doi.org/10.1021/jp509659p>.
41. D. Pacilé, J.C. Meyer, A. Fraile Rodríguez, M. Papagno, C. Gómez-Navarro, R.S. Sundaram, M. Burghard, K. Kern, C. Carbone and U. Kaiser, *Carbon*, **49**, 966 (2011); <https://doi.org/10.1016/j.carbon.2010.09.063>.
42. D. Pandey, R. Reifengerger and R. Piner, *Surf. Sci.*, **602**, 1607 (2008); <https://doi.org/10.1016/j.susc.2008.02.025>.
43. C.K. Chua and M. Pumera, *Chem. Soc. Rev.*, **43**, 291 (2014); <https://doi.org/10.1039/C3CS60303B>.
44. I.K. Moon, J. Lee, R.S. Ruoff and H. Lee, *Nat. Commun.*, **1**, 1 (2010); <https://doi.org/10.1038/ncomms1067>.
45. C.K. Chua, A. Ambrosi and M. Pumera, *J. Mater. Chem.*, **22**, 11054 (2012); <https://doi.org/10.1039/c2jm16054d>.
46. F. Tuinstra and J.L. Koenig, *J. Chem. Phys.*, **53**, 1126 (1970); <https://doi.org/10.1063/1.1674108>.
47. Y. Si and E.T. Samulski, *Nano Lett.*, **8**, 1679 (2008); <https://doi.org/10.1021/nl080604h>.
48. S. Stankovich, R.D. Piner, S.T. Nguyen and R.S. Ruoff, *Carbon*, **44**, 3342 (2006); <https://doi.org/10.1016/j.carbon.2006.06.004>.
49. C.K. Chua and M. Pumera, *J. Mater. Chem. A*, **1**, 1892 (2013); <https://doi.org/10.1039/C2TA00665K>.
50. E.H. Lieb, *Phys. Rev. Lett.*, **62**, 1201 (1989); <https://doi.org/10.1103/PhysRevLett.62.1201>.
51. D.W. Boukhvalov, *Phys. Chem. Chem. Phys.*, **12**, 15367 (2010); <https://doi.org/10.1039/c0cp01009j>.
52. D.W. Boukhvalov, *RSC Adv.*, **3**, 7150 (2013); <https://doi.org/10.1039/c3ra23372c>.
53. E.J.G. Santos, A. Ayuela and D. Sánchez-Portal, *New J. Phys.*, **14**, 043022 (2012); <https://doi.org/10.1088/1367-2630/14/4/043022>.
54. M. Wang, W. Huang, M.B. Chan-Park and C.M. Li, *Nanotechnology*, **22**, 105702 (2011); <https://doi.org/10.1088/0957-4484/22/10/105702>.
55. T. Tang, N. Tang, Y. Zheng, X. Wan, Y. Liu, F. Liu, Q. Xu and Y. Du, *Sci. Rep.*, **5**, 8848 (2015); <https://doi.org/10.1038/srep08448>.
56. T. Tang, F. Liu, Y. Liu, X. Li, Q. Xu, Q. Feng, N. Tang and Y. Du, *Appl. Phys. Lett.*, **104**, 123104 (2014); <https://doi.org/10.1063/1.4869827>.
57. S.C. Ray, N. Soin, T. Makgato, C.H. Chuang, W.F. Pong, S.S. Roy, S.K. Ghos, A.M. Strydom and J.A. McLaughlin, *Sci. Rep.*, **4**, 3862 (2014); <https://doi.org/10.1038/srep03862>.
58. K.A. Mkhoyan, A.W. Contryman, J. Silcox, D.A. Stewart, G. Eda, C. Mattevi, S. Miller and M. Chhowalla, *Nano Lett.*, **9**, 1058 (2009); <https://doi.org/10.1021/nl8034256>.
59. A. Lerf, H. He, M. Forster and J. Klinowski, *J. Phys. Chem. B*, **102**, 4477 (1998); <https://doi.org/10.1021/jp9731821>.
60. W.W. Cai, R.D. Piner, F.J. Stadermann, S. Park, M.A. Shaibat, Y. Ishii, D.X. Yang, A. Velamakanni, S.J. An, M. Stoller, J. An, D. Chen and R.S. Ruoff, *Science*, **321**, 1815 (2008); <https://doi.org/10.1126/science.1162369>.

61. H. Kumazaki and D. S. Hirashima, *J. Phys. Soc. Jpn.*, **77**, 044705 (2008); <https://doi.org/10.1143/JPSJ.77.044705>.
62. S. Bhowmick and V.B. Shenoy, *J. Chem. Phys.*, **128**, 244717 (2008); <https://doi.org/10.1063/1.2943678>.
63. H. Lee, Y.-W. Son, N. Park, S. Han and J. Yu, *Phys. Rev. B*, **72**, 174431 (2005); <https://doi.org/10.1103/PhysRevB.72.174431>.
64. S. Banerjee, M. Sardar, N. Gayathri, A.K. Tyagi and B. Raj, *Phys. Rev. B*, **72**, 075418 (2005); <https://doi.org/10.1103/PhysRevB.72.075418>.
65. S. Banerjee, M. Sardar, N. Gayathri, A.K. Tyagi and B. Raj, *Appl. Phys. Lett.*, **88**, 062111 (2006); <https://doi.org/10.1063/1.2166697>.
66. S. Panigrahi, A. Bhattacharya, D. Bandyopadhyay, S.J. Grabowski, D. Bhattacharyya and S. Banerjee, *J. Phys. Chem. C*, **115**, 14819 (2011); <https://doi.org/10.1021/jp2027466>.
67. K. Bagani, M.K. Ray, B. Satpati, N.R. Ray, M. Sardar and S. Banerjee, *J. Phys. Chem. C*, **118**, 13254 (2014); <https://doi.org/10.1021/jp503034d>.
68. K. Bagani, A. Bhattacharya, J. Kaur, A. Rai Chowdhury, B. Ghosh, M. Sardar and S. Banerjee, *J. Appl. Phys.*, **115**, 023902 (2014); <https://doi.org/10.1063/1.4861173>.
69. Y.F. Wang, S.B. Singh, M.V. Limaye, Y.C. Shao, S.H. Hsieh, L.Y. Chen, H.C. Hsueh, H.T. Wang, J.W. Chiou, Y.C. Yeh, C.W. Chen, C.H. Chen, S.C. Ray, J. Wang, W.F. Pong, Y. Takagi, T. Ohigashi, T. Yokoyama and N. Kosugi, *Sci. Rep.*, **5**, 15439 (2015); <https://doi.org/10.1038/srep15439>.
70. M.D. Mukadam and S.M. Yusuf, *Physica B*, **403**, 2602 (2008); <https://doi.org/10.1016/j.physb.2008.01.022>.
71. A.N. Andriotis, R. Michael Sheetz and M. Menon, *J. Phys. Condens. Matter*, **22**, 334210 (2010); <https://doi.org/10.1088/0953-8984/22/33/334210>.
72. Z.H. Zhu, D.Q. Gao, Z.L. Yang, J. Zhang, Z.H. Shi, Z.P. Zhang and D.S. Xue, *Mod. Phys. Lett. B*, **27**, 1350031 (2013); <https://doi.org/10.1142/S0217984913500310>.